Letter

Intermode coupling in nanomechanical resonators as a key for tuning the effective nonlinearity

Andrey A. Shevyrin[1,2,*] Arthur G. Pogosov[1,3] Askhat K. Bakarov[1,3]
Alexander A. Shklyaev[1,3] and Akshay Naik[2]

[1] *Rzhanov Institute of Semiconductor Physics SB RAS, 13 Lavrentyeva ave., Novosibirsk 630090, Russia*
[2] *Centre for Nano Science and Engineering, Indian Institute of Science Bangalore, Karnataka 560012, India*
[3] *Novosibirsk State University, 2 Pirogova str., Novosibirsk 630090, Russia*

(Received 30 July 2024; revised 25 November 2024; accepted 3 December 2024; published 23 December 2024)

Nonlinear interaction of flexural and torsional modes is experimentally studied in a cantileverlike nanomechanical resonator. The resonant frequency of each mode depends much weaker on its own amplitude than on the amplitude of another mode. This property makes it possible to widely tune the effective nonlinearity of each mode on chip, making the same system exhibit hardening, softening, or linear behavior. This nonlinear tuning in one mode is achieved by adjusting the driving frequency and amplitude of the other mode. It is shown that this effective tunability may be characteristic of resonators with a high width-to-thickness ratio.

DOI: 10.1103/PhysRevApplied.22.L061003

Artificially created micro- and nanomechanical resonators demonstrate a plethora of classical, quantum, linear, and nonlinear phenomena [1,2] and are useful for sensing various physical quantities [3,4]. Their single degree-of-freedom operation has led to many interesting effects and continues to be an active area of research [5–7]. Nanomechanical resonators are characterized by their tendency to enter the nonlinear regime at relatively low amplitudes [8]. This characteristic leads to a diverse dynamic response in these devices, including phenomena such as parametric resonance, multistability, and chaotic motion [9–12]. These effects are significant both from a fundamental research perspective and for potential practical applications. A notable example is the behavior of nonlinear oscillators near the quantum ground state [13]. However, these nonlinearities also present a considerable challenge in the use of nanomechanical resonators as sensors by restricting their dynamic range. Thus, it is crucial to understand the source of these nonlinearities and develop methods to control them [14,15].

When several oscillatory modes are coupled, the range of the effects displayed expands even more [2,16,17]. Linear coupling between the modes leads to hybridization and anticrossings [18–20]. Nonlinear effects make it possible to cool or amplify oscillatory modes by parametric pumping at the frequency difference or sum [21] and to generate squeezed states [22]. The mode coupling is also useful for applications, such as phononic frequency combs [23,24] and multimode sensing, which can be used to gain more information and thus to improve the resolution in atomic force microscopy [25] among others.

Due to intermode nonlinearity, the one (controlling) mode can influence the resonant frequencies of other (controlled) modes. This provides a way for *in situ* frequency tuning and detection of the modes that otherwise go undetected due to bandwidth limitations [26]. The use of nonlinear coupling has also been suggested for quantum nondemolition measurements [27] and for the generation of phononic combs [28]. However, often (although not always [29]) the intermode nonlinearity is weaker than or of the same order as the intramode coupling. This implies that to shift the frequency of the controlled mode by its resonance width, the controlling mode must be driven to amplitudes that exceed the intramode nonlinearity threshold [30–32].

This dispersive coupling is commonly observed between flexural oscillations and studied in doubly clamped beams [26,31–33], where its origin is the same as that of intramode nonlinearity, namely, the oscillation-induced tension. This physical mechanism is absent in single-clamped cantilevers, where experiment diverges from theory even when intramode nonlinearity is studied [34,35]. In addition, interaction between the modes other than flexural may open unexplored areas of research [30]. Such interaction, desirable or not, is especially relevant for multimode sensors, because the more dissimilar the modes are, the more benefits can be expected from switching to the multimode operation. In addition, it is the cantilevered resonators that are commonly used in microscopy.

In the present paper, we show that the nonlinear coupling between flexural and torsional modes in flat

*Contact author: shevandrey@isp.nsc.ru

 © 2024 American Physical Society

cantileverlike resonators can be much stronger than the intramode nonlinearity. Because of that, the effective nonlinearity of each mode is tunable and controlled by another mode, with the driving frequency of the latter determining whether the system displays hardening, softening, or linear behavior. This method for *in situ* nonlinearity tuning is advantageous in comparison to geometry adjustment [36], which is permanent, and electrostatic tuning [14,15], which, determined by a gate voltage squared, is unidirectional (the induced change in the nonlinearity coefficients cannot be reversed in situ).

Experimental samples are created from a GaAs/(Al, Ga)As heterostructure containing a 400-nm-thick sacrificial $Al_{0.8}Ga_{0.2}As$ layer 166 nm below the surface and a two-dimensional electron gas (2DEG) centered at the depth of 88 nm. The samples are made using electron-beam lithography followed by plasma-chemical etching. The sacrificial layer is selectively etched from under the resonators using HF aqueous solution.

One of the samples is shown in Fig. 1(a). It represents a multielectrode system sustaining multiple mechanical modes shown in Fig. 1(b). One of the electrodes is a suspended bridge (grounded in the experiments) with a wide circular central part. Near one of its clamped edges, shallow plasma-chemically etched trenches form a 2DEG constriction used to detect mechanical oscillations by measuring its conductance as described below. The bridge

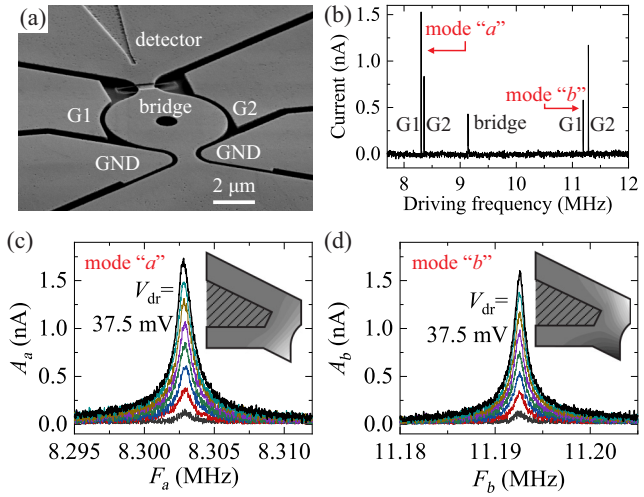

FIG. 1. (a) SEM image of one of the studied samples. The electrodes labeled "G1," "G2," and "bridge" play the role of mechanical resonators. The electrodes labeled "GND" are grounded. (b) Coarse frequency sweep displaying the observed mechanical modes. (c),(d) Frequency sweeps in the vicinity of modes "*a*" and "*b*" measured at various amplitudes driving voltage amplitudes V_{dr} (2.5:5:37.5 mV). Insets: simulated mode shapes of the gates "G1" and "G2." Color shows the signed displacement. The stripped regions are nonsuspended and immobile; the background color in these regions corresponds to zero displacement.

is surrounded by four side gates. Two of them (labeled "GND") were grounded and played no role in the experiment, while the electrodes labeled "G1" and "G2" were used as gates and resonators at the same time. We first discuss single-tone driving of mechanical oscillations implemented by applying the same sum $V_{dc} + V_{dr}\cos(2\pi Ft)$ of dc and ac voltages to gates "G1" and "G2" [37–39] ($V_{dc} = -7$ V in all the measurements described). Between the detector terminals, an ac voltage $V_{SD}\cos[2\pi(F - f_{dm})t]$ was applied ($V_{SD} = 14$ mV), where $f_{dm} = 9.14$ kHz is the heterodyne down-mixing frequency. The oscillations are detected by measuring the current flowing through the constriction at frequency f_{dm} using the lock-in technique. This current is proportional to the amplitude of oscillation and sensitive to their phase [37,40]. We do not calibrate the response with respect to displacement and express the oscillation amplitudes in nA units. The measurements were done at the temperature of 7 K, with the sample in vacuum.

Figure 1(b) shows the measured signal vs driving frequency F. Five resonant modes are seen: two pairs at 8.3 and 11.25 MHz, and one single resonance at 9.1 MHz. Using a laser Doppler vibrometer, we found that the paired resonances appear because of mechanical oscillations of gates "G1" and "G2," while the single resonance originates from the bridge oscillations. In the rest of the paper, we focus on the modes labeled "*a*" and "*b*" in Fig. 1(b). They belong to the same gate and, as we show below, they display intermode interaction. None of them interact with any other mode. The other two gate modes also interact with each other in a similar way.

Figures 1(c) and 1(d) show detailed frequency sweeps of resonances "*a*" and "*b*" measured at various driving amplitudes V_{dr}. The quality factors extracted from the experiment are $Q_a = 10\,600$ and $Q_b = 11\,400$. The insets illustrate the modal shapes calculated using finite-element modeling. The color shows the out-of-plane displacement. Most of the gate area remains immobile (dark gray regions), apart from the right corners. In the left inset, the modal displacement is positive only (brighter region), while, in the right one, its sign alternates and both darker and brighter regions are seen. Thus, modes "*a*" and "*b*" are flexural and torsional, respectively. Conductance of the 2DEG constriction is sensitive to displacement of the gates biased by V_{dc}, because of a change in the gate-constriction capacitance and, hence, electron density.

Hereinafter we consider the effects observed when the two modes are driven simultaneously. The universally expected behavior can be derived from the perturbation theory applied to an arbitrary hamiltonian of a nonlinear system having 2 degrees of freedom (the displacements corresponding to normal modes "*a*" and "*b*" from a potential minimum). The expected shifts of the resonant frequencies are quadratic (in the first nonzero order) with respect to amplitudes of both modes A_a, A_b:

$$f_i = f_{0i} + \sum_{j=a,b} \alpha_{ij} A_j^2 + \ldots, \tag{1}$$

where amplitudes A_i obey the following equation:

$$A_i = A_{0i} \frac{f_i}{\sqrt{4Q_i^2 (F_i - f_i)^2 + {f_i}^2}}. \tag{2}$$

Here indices i,j denote the mode and take values "a" and "b." Coefficients α_{aa}, α_{bb} and α_{ab}, α_{ba} characterize intra- and intermode nonlinearities, respectively. The mutual influence of the modes can be shown to be symmetric:

$$m_a f_{oa} \alpha_{ab} = m_b f_{ob} \alpha_{ba}, \tag{3}$$

where m_a and m_b are the modal effective masses.

In the experiment, the two modes were driven by applying two-tone voltage $V_{\rm dc} + V_a \cos(2\pi F_a t) + V_b \cos(2\pi F_b t)$ to gates "G1" and "G2." To detect the modes, voltage $V_{\rm SD} \cos[2\pi (F_a - f_{\rm dma})t] + V_{\rm SD} \cos[2\pi (F_b - f_{\rm dmb})t]$ was applied between the terminals of the 2DEG constriction. The oscillation amplitudes $A_{\rm a}, A_{\rm b}$ (in nA units) were measured at down-mixing frequencies $f_{\rm dma} = 9.14$ kHz, $f_{\rm dmb} = 11.13$ kHz at the same time. Thus, the modes were detected simultaneously at different, well-separated pairs of driving and down-mixing frequencies.

In Fig. 2, the left and right columns of plots show the results of two separate sets of measurements. The left column illustrates how mode "b" (controlling mode) influences mode "a" (the controlled mode whose amplitude is displayed). In the right column, the controlled and controlling modes are swapped. The driving amplitudes of the controlled and controlling modes are 10 mV (unless otherwise specified) and 30 mV, respectively.

Figures 2(a) and 2(b) show how the controlled mode frequency depends on its driving frequency (plotted along the horizontal axes) at various driving frequencies of the controlling mode (indicated next to the curves). In Figs. 2(c) and 2(d), the color displays the squared amplitude of the controlled mode as a function of both driving frequencies F_a and F_b. As we show below, the controlling mode influences two parameters of the controlled one, namely, the resonant frequency and the effective nonlinearity.

When the controlling mode [whose driving frequency is plotted along the vertical axes in Figs. 2(c) and 2(d)] is driven far from the resonance and its amplitude is small, the resonant frequency of the controlled mode is constant, and its amplitude-frequency curves [the top and bottom ones in Figs. 2(a) and 2(b)] display symmetric Lorentzian shapes showing that the oscillations are linear. When the controlling mode is resonantly driven, the eigenfrequency of the controlled mode increases, i.e., the intermode interaction can be used to tune the resonant frequencies in our

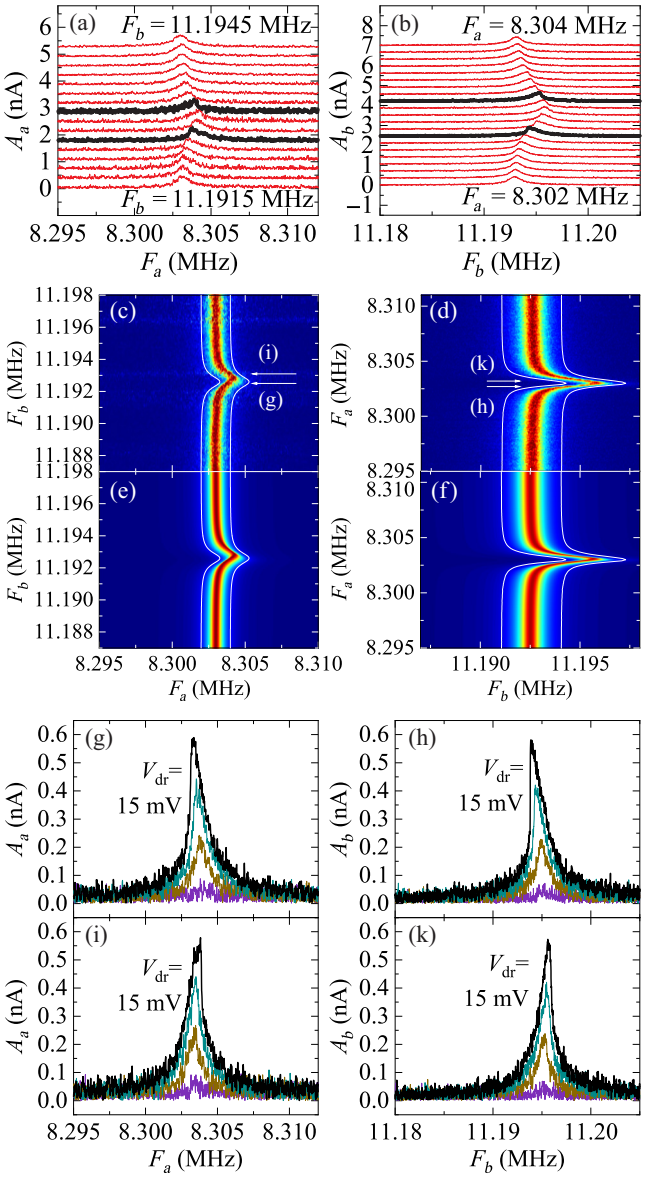

FIG. 2. (a),(b) Amplitude vs driving frequency of the controlled modes (plotted along the horizontal axis) at various driving frequencies of the controlling modes (shown next to the curves). The curves displaying the most prominent nonlinearity are bold. (c),(d) The measured squared amplitude (color) of the modes as a function of both driving frequencies. The arrows correspond to the bold curves in (a),(b). (e),(f) Same results as in (c),(d), but simulated rather than measured. (g)–(k) Same results as displayed by the bold curves in (a),(b), but measured at various driving amplitudes of the controlled modes (3:4:15 mV).

system. Apart from that, the displayed Lorentzian bells are tilted, with the tilting direction determined by the sign of the controlling frequency detuning from the resonance. In Figs. 2(g)–2(k), this behavior is illustrated at various amplitudes of the controlled mode. At $V_{\rm dr} = 15$ mV, the amplitudes are close to the critical ones (one of the resonance slopes is nearly vertical), while, if the modes are driven individually [see Fig. 1(c) and 1(d)], driving

amplitudes of more than 2 times higher than this value do not lead to any noticeable tilting.

We fit the tilted $A_a(F_a)$ and $A_b(F_b)$ curves (each measured at a fixed driving frequency of the controlling mode and driving amplitudes of both modes) by the implicit dependences described by Eq. (2), where resonant frequency f_i of the controlled mode is assumed to depend on its own amplitude as

$$f_i = f_i|_{A_i\to 0} + \alpha_i A_i^2. \tag{4}$$

Coefficients $f_i|_{A_i\to 0}$ (the small-amplitude resonant frequency) and α_i (the effective nonlinearity coefficient describing the tilting degree) are derived from the fitting.

It is clear from Eq. (1) that the former coefficient should depend linearly on the squared amplitude of the controlling mode and display the same dependence on its driving frequency:

$$f_a|_{A_a\to 0} = f_{0a} + \alpha_{ab} A_b^2|_{A_a\to 0}, \tag{5}$$

$$f_b|_{A_b\to 0} = f_{0b} + \alpha_{ba} A_a^2|_{A_b\to 0}, \tag{6}$$

Controlling mode amplitudes $A_a|_{A_b\to 0}$ and $A_b|_{A_a\to 0}$ were measured when the controlled modes were far from their resonances, the expected behavior was experimentally confirmed, and the values of tunability coefficients $\alpha_{ab} = 747$ Hz/nA^2 and $\alpha_{ba} = 1.885$ kHz/nA^2 were determined. The white lines displayed in Figs. 2(c)–2(f) are the measured dependences of the right-hand sides of Eqs. (5) and (6) on the driving frequencies of the controlling mode, horizontally shifted by ± 1 and ± 1.5 kHz for clarity.

We could naively derive the expected behavior of coefficients α_a, α_b as well from the explicitly written terms of Eqs. (1) and (2) by taking into account A_b dependence on A_a via f_b:

$$\alpha_a = \frac{\mathrm{d}\Delta f_a}{\mathrm{d}(A_a^2)} = \alpha_{aa} + 4\alpha_{ab}\alpha_{ba}\frac{Q_b}{f_{0b}} A_{bx} A_{by} + \ldots, \tag{7}$$

where $A_{bx} = A_{0b} p_b/(1+p_b^2)$, $A_{by} = A_{0b}/(1+p_b^2)$ are the components of the amplitude in and out of phase with respect to the driving force, $p_b = 2Q_b(F_b - f_{0b})/f_{0b}$ is the dimensionless frequency detuning from the resonance. The equation for α_b results from swapping indices "a" and "b" in Eq. (7). However, in a general case, this approach would be wrong. To obtain an equation for α_i correct up to the second order, terms of the fourth order in amplitudes A_{0i} has to be written explicitly in Eq. (1) when deriving it from the hamiltonian using the perturbation theory [41]. The resulting equation would include additional terms, such as those proportional to A_b^2, omitted in Eq. (7). Nonetheless, Eq. (7) describes our experiment well, which means that the omitted terms are small.

The effective nonlinearity coefficients α_i derived from fitting $A_a(F_a)$ and $A_b(F_b)$ curves using Eqs. (2), (4) at various driving frequencies of the controlling mode are shown in Figs. 3(a) and 3(b) by the black squares. The red curves display $4\alpha_{ab}\alpha_{ba}Q_b A_{bx} A_{by}/f_{0b}$ (left plot) and $4\alpha_{ab}\alpha_{ba}Q_a A_{ax} A_{ay}/f_{0a}$ (right plot) values, also extracted from the experiment. These curves fit well the experimental α_i values, and this agrees with the description above and with Eq. (7) in particular.

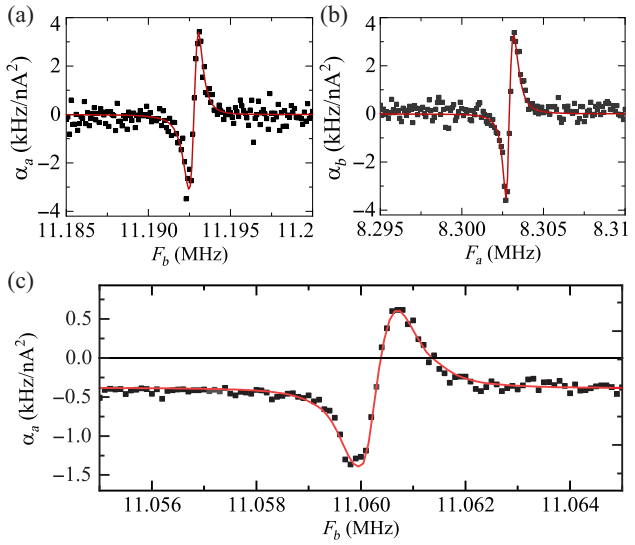

FIG. 3. (a),(b) The black squares show the coefficients characterizing the degree of nonlinearity of the controlled modes as functions of the driving frequency of the controlling modes. The dependences fit to the measured product of the in-phase and out-of-phase components of the controlling mode amplitude (red curves). Since far from the controlling mode resonance, the data points tend to zero, the intramode nonlinearity is much weaker than the intermode one. (c) The data measured on another sample displaying a measurable intramode nonlinearity, which can be compensated by the intermode one.

The data points in Figs. 3(a) and 3(b) lie on S-like curves deserving special attention. First, when the controlling mode is driven far from its resonance, nonlinearity coefficients α_i tend to zero, showing that coefficients α_{aa}, α_{bb} are also close to zero and the intramode nonlinearity is weak. Second, resonant driving of the controlling mode drastically changes the effective nonlinearity coefficients α_a, α_b, showing that the intermode nonlinearity is strong. Third, coefficients α_a, α_b can be made both positive and negative, allowing nonlinearity tuning in wide limits from softening to hardening.

Qualitatively, the influence of intermode coupling on the effective nonlinearity can be explained by the back action of the controlled mode on the controlling one, tuning or detuning the latter from the driving frequency and, thus increasing or decreasing its amplitude, which, in turn, modifies the resonant frequency of the controlled mode.

Not all of the studied samples displayed weak intramode nonlinearity. For example, the data points measured on another sample and shown in Fig. 3(c) fall on an S-like

curve centered vertically at a nonzero value. In this case, the intermode coupling makes it possible to compensate the intramode nonlinearity by adjusting the driving frequency of the controlling mode and minimizing its effective coefficient α_a.

By substituting the experimentally determined values of α_{ab} and α_{ba} and $\alpha_{aa} = \alpha_{bb} = 0$ into Eqs. (1), (2), we simulate the squared amplitude dependences on both driving frequencies F_a, F_b [see Figs. 2(e) and 2(f)] and also see good agreement between the theory and experiment [Figs. 2(c) and 2(d)]. In these plots, the effective nonlinearity is seen as the vertical shift of the dark red regions, where the amplitude is maximal, with respect to the bright regions of small amplitude enveloped by the white solid lines.

One of the physical mechanisms that may cause the coupling between flexural and torsional modes [30] can be illustrated on the example of a more common and simple case, namely, a thin cantilever beam. The local flexural rigidity of such a beam is determined by the second moment of inertia $I_{yy} = \int\int y^2 \mathrm{d}x\mathrm{d}y$, where the integral is taken over the cross section with width W and thickness t. If the cross section is twisted by angle ϕ, then $I_{yy} = Wt\left[t^2 + \left(W^2 - t^2\right)\sin^2\phi\right]/12$, i.e., if $W > t$, the twisting increases the second moment of inertia, the local rigidity of the beam and the flexural resonant frequency, like in our experiment. Due to the symmetry expressed by Eq. (3), the flexural motion should also increase the torsional resonant frequency. Thus, the proposed microscopic explanation agrees with the signs of the frequency shifts observed experimentally. One conclusion that can be drawn is that strong intermode coupling is expected in flat resonators where $W \gg t$ (in our samples $W/t \approx 30$). Finally, it should be noticed that, although we believe that the proposed mechanism is most likely responsible for the strong intermode coupling in our case, some additional features may be expected because of the special shape of the gate resonators, clearly different from that of a thin cantilever. Also, strictly speaking, electrostatic nonlinearity can contribute to the intermode coupling. This contribution could be revealed by more detailed measurements at various dc gate voltages, however, this study goes beyond the scope of the present letter.

To conclude, we experimentally show that the effective nonlinearity displayed by an oscillatory (controlled) mode of a nanomechanical resonator can be tuned on chip in a wide range by driving another (controlling) mode of the same resonator. Depending on detuning of the latter from the resonance, the effective nonlinearity coefficient can be set to both positive and negative values, making the system to display either hardening or softening on demand. The system created exhibits intramode nonlinearity much weaker than the intermode ones; the nonlinear regime controllably induced by driving both modes is reached at the amplitudes so small that, if the modes are driven with the same amplitudes individually, their oscillations are deeply linear. In another sample, we show that the intramode nonlinearity can be compensated by the intermode interaction. Finally, we show that strong intermode coupling may be caused by a high wide-to-thickness ratio and, thus, it can be reproduced and generalized in resonators of other types.

Acknowledgments. The work is supported by Russian Science Foundation (Grant No. 22-12-00343 – fabrication of the experimental samples, preliminary measurements and data analysis), the Ministry of Science and Higher Education of The Russian Federation (Project No. FWGW-2022-0011 – characterization of the initial heterostructures), and the International Visiting Faculty Programme at Indian Institute of Science (measurements). The authors acknowledge core facilities "VTAN" (Novosibirsk State University) for access to electron-beam lithography equipment. The authors are grateful to Dr. Praveen Kumar and Professor Gayathri Pillai for providing access to the laser Doppler vibrometer and assistance in carrying out the measurements. A.A.S. is grateful to Alexey Nenashev for a fruitful discussion.

[1] B. Xu, P. Zhang, J. Zhu, Z. Liu, A. Eichler, X.-Q. Zheng, J. Lee, A. Dash, S. More, S. Wu, Y. Wang, H. Jia, A. Naik, A. Bachtold, R. Yang, P. X.-L. Feng, and Z. Wang, Nanomechanical resonators: Toward atomic scale, ACS Nano **16**, 15545 (2022).

[2] A. Bachtold, J. Moser, and M. I. Dykman, Mesoscopic physics of nanomechanical systems, Rev. Mod. Phys. **94**, 045005 (2022).

[3] S. L. de Bonis, C. Urgell, W. Yang, C. Samanta, A. Noury, J. Vergara-Cruz, Q. Dong, Y. Jin, and A. Bachtold, Ultrasensitive displacement noise measurement of carbon nanotube mechanical resonators, Nano Lett. **18**, 5324 (2018).

[4] M. Yuksel, E. Orhan, C. Yanik, A. B. Ari, A. Demir, and M. S. Hanay, Nonlinear nanomechanical mass spectrometry at the single-nanoparticle level, Nano Lett. **19**, 3583 (2019).

[5] S. Schmid, L. G. Villanueva, and M. L. Roukes, *Fundamentals of Nanomechanical Resonators* (Springer International Publishing, Springer Cham, 2023).

[6] H. Yamaguchi, GaAs-based micro/nanomechanical resonators, Semicond. Sci. Technol. **32**, 103003 (2017).

[7] A. G. Pogosov, A. A. Shevyrin, D. A. Pokhabov, E. Y. Zhdanov, and S. Kumar, Suspended semiconductor nanostructures: Physics and technology, J. Phys.: Condens. Matter **34**, 263001 (2022).

[8] N. J. Engelsen, A. Beccari, and T. J. Kippenberg, Ultrahigh-quality-factor micro- and nanomechanical resonators using dissipation dilution, Nat. Nanotechnol. **19**, 725 (2024).

[9] J. S. Ochs, D. K. J. Boneß, G. Rastelli, M. Seitner, W. Belzig, M. I. Dykman, and E. M. Weig, Frequency comb from a single driven nonlinear nanomechanical mode, Phys. Rev. X **12**, 041019 (2022).

[10] R. B. Karabalin, M. C. Cross, and M. L. Roukes, Nonlinear dynamics and chaos in two coupled nanomechanical resonators, Phys. Rev. B **79**, 165309 (2009).

[11] R. Karabalin, in *Encyclopedia of Nanotechnology*, edited by B. Bhushan (Springer Netherlands, Dordrecht, 2014), p. 1.
[12] I. Mahboob and H. Yamaguchi, Bit storage and bit flip operations in an electromechanical oscillator, Nat. Nanotechnol. **3**, 275 (2008).
[13] C. Samanta, S. L. De Bonis, C. B. Møller, R. Tormo-Queralt, W. Yang, C. Urgell, B. Stamenic, B. Thibeault, Y. Jin, D. A. Czaplewski, F. Pistolesi, and A. Bachtold, Nonlinear nanomechanical resonators approaching the quantum ground state, Nat. Phys. **19**, 1340 (2023).
[14] I. Kozinsky, H. W. C. Postma, I. Bargatin, and M. L. Roukes, Tuning nonlinearity, dynamic range, and frequency of nanomechanical resonators, Appl. Phys. Lett. **88**, 253101 (2006).
[15] C. Samanta, N. Arora, and A. K. Naik, Tuning of geometric nonlinearity in ultrathin nanoelectromechanical systems, Appl. Phys. Lett. **113**, 113101 (2018).
[16] A. Hajjaj, N. Jaber, S. Ilyas, F. Alfosail, and M. Younis, Linear and nonlinear dynamics of micro and nano-resonators: Review of recent advances, Int. J. Non. Linear Mech. **119**, 103328 (2020).
[17] M.-L. Guo, J.-W. Fang, J.-F. Chen, B.-L. Li, H. Chen, Q. Zhou, Y. Wang, H.-Z. Song, K. Y. Arutyunov, G.-C. Guo, Z.-M. Wang, and G.-W. Deng, Mode coupling in electromechanical systems: Recent advances and applications, Adv. Electron. Mater. **9**, 2201305 (2023).
[18] P. Prasad, N. Arora, and A. K. Naik, Gate tunable cooperativity between vibrational modes, Nano Lett. **19**, 5862 (2019), pMID: 31408355.
[19] T. Faust, J. Rieger, M. J. Seitner, P. Krenn, J. P. Kotthaus, and E. M. Weig, Nonadiabatic dynamics of two strongly coupled nanomechanical resonator modes, Phys. Rev. Lett. **109**, 037205 (2012).
[20] I. Mahboob, M. Villiers, K. Nishiguchi, D. Hatanaka, A. Fujiwara, and H. Yamaguchi, A correlated electromechanical system, New J. Phys. **19**, 033026 (2017).
[21] W. J. Venstra, H. J. R. Westra, and H. S. J. van der Zant, Q-factor control of a microcantilever by mechanical sideband excitation, Appl. Phys. Lett. **99**, 151904 (2011).
[22] I. Mahboob, H. Okamoto, K. Onomitsu, and H. Yamaguchi, Two-mode thermal-noise squeezing in an electromechanical resonator, Phys. Rev. Lett. **113**, 167203 (2014).
[23] A. Ganesan, C. Do, and A. Seshia, Phononic frequency comb via intrinsic three-wave mixing, Phys. Rev. Lett. **118**, 033903 (2017).
[24] J. Sun, S. Yu, H. Zhang, D. Chen, X. Zhou, C. Zhao, D. D. Gerrard, R. Kwon, G. Vukasin, D. Xiao, T. W. Kenny, X. Wu, and A. Seshia, Generation and evolution of phononic frequency combs via coherent energy transfer between mechanical modes, Phys. Rev. Appl. **19**, 014031 (2023).
[25] R. Garcia and E. T. Herruzo, The emergence of multifrequency force microscopy, Nat. Nanotechnol. **7**, 217 (2012).
[26] A. B. Arı, M. Çağatay Karakan, C. Yanık, İ. İ. Kaya, and M. Selim Hanay, Intermodal coupling as a probe for detecting nanomechanical modes, Phys. Rev. Appl. **9**, 034024 (2018).
[27] D. H. Santamore, A. C. Doherty, and M. C. Cross, Quantum nondemolition measurement of Fock states of mesoscopic mechanical oscillators, Phys. Rev. B **70**, 144301 (2004).
[28] Z. Qi, C. R. Menyuk, J. J. Gorman, and A. Ganesan, Existence conditions for phononic frequency combs, Appl. Phys. Lett. **117**, 183503 (2020).
[29] I. Mahboob, N. Perrissin, K. Nishiguchi, D. Hatanaka, Y. Okazaki, A. Fujiwara, and H. Yamaguchi, Dispersive and dissipative coupling in a micromechanical resonator embedded with a nanomechanical resonator, Nano Lett. **15**, 2312 (2015).
[30] H. Westra, H. van der Zant, and W. Venstra, Modal interactions of flexural and torsional vibrations in a microcantilever, Ultramicroscopy **120**, 41 (2012).
[31] M. H. Matheny, L. G. Villanueva, R. B. Karabalin, J. E. Sader, and M. L. Roukes, Nonlinear mode-coupling in nanomechanical systems, Nano Lett. **13**, 1622 (2013).
[32] W. J. Venstra, R. van Leeuwen, and H. S. J. van der Zant, Strongly coupled modes in a weakly driven micromechanical resonator, Appl. Phys. Lett. **101**, 243111 (2012).
[33] H. J. R. Westra, M. Poot, H. S. J. van der Zant, and W. J. Venstra, Nonlinear modal interactions in clamped-clamped mechanical resonators, Phys. Rev. Lett. **105**, 117205 (2010).
[34] L. G. Villanueva, R. B. Karabalin, M. H. Matheny, D. Chi, J. E. Sader, and M. L. Roukes, Nonlinearity in nanomechanical cantilevers, Phys. Rev. B **87**, 024304 (2013).
[35] J. E. Sader, S. Stassi, C. Ricciardi, and M. L. Roukes, Effect of intramodal and intermodal nonlinearities on the flexural resonant frequencies of cantilevered beams, Phys. Rev. B **108**, 224303 (2023).
[36] L. L. Li, P. M. Polunin, S. Dou, O. Shoshani, B. Scott Strachan, J. S. Jensen, S. W. Shaw, and K. L. Turner, Tailoring the nonlinear response of MEMS resonators using shape optimization, Appl. Phys. Lett. **110**, 081902 (2017).
[37] A. A. Shevyrin, A. G. Pogosov, M. V. Budantsev, A. K. Bakarov, A. I. Toropov, E. E. Rodyakina, and A. A. Shklyaev, Actuation and transduction of resonant vibrations in GaAs/AlGaAs-based nanoelectromechanical systems containing two-dimensional electron gas, Appl. Phys. Lett. **106**, 183110 (2015).
[38] A. A. Shevyrin, A. G. Pogosov, A. K. Bakarov, and A. A. Shklyaev, Piezoelectric electromechanical coupling in nanomechanical resonators with a two-dimensional electron gas, Phys. Rev. Lett. **117**, 017702 (2016).
[39] A. A. Shevyrin, A. G. Pogosov, A. K. Bakarov, and A. A. Shklyaev, Electrostatic actuation and charge sensing in piezoelectric nanomechanical resonators with a two-dimensional electron gas, Appl. Phys. Lett. **118**, 183105 (2021).
[40] I. Bargatin, E. B. Myers, J. Arlett, B. Gudlewski, and M. L. Roukes, Sensitive detection of nanomechanical motion using piezoresistive signal downmixing, Appl. Phys. Lett. **86**, 133109 (2005).
[41] See Supplemental Material at http://link.aps.org/supplemental/10.1103/PhysRevApplied.22.L061003 for the calculation details.